Mid-Infrared Spectrometer Using Opto-Nanofluidic Slot-Waveguide for Label-Free On-Chip Chemical Sensing

Pao Tai Lin,*,[†] Sen Wai Kwok,[‡] Hao-Yu Greg Lin,[§] Vivek Singh,[†] Lionel C. Kimerling,[†] George M. Whitesides,[‡] and Anu Agarwal[†]

[†]Microphotonics Center, Massachusetts Institute of Technology, 77 Massachusetts Avenue, Cambridge, Massachusetts 02139, United States

[‡]Department of Chemistry and Chemical Biology, Harvard University, 12 Oxford Street, Cambridge, Massachusetts 02138, United States

[§]Center for Nanoscale Systems, 11 Oxford Street, Cambridge, Massachusetts 02138, United States

S *Supporting Information*

ABSTRACT: A mid-infrared (mid-IR) spectrometer for label-free on-chip chemical sensing was developed using an engineered nanofluidic channel consisting of a Si-liquid-Si slot-structure. Utilizing the large refractive index contrast ($\Delta n \sim 2$) between the liquid core of the waveguide and the Si cladding, a broadband mid-IR lightwave can be efficiently guided and confined within a nanofluidic capillary (≤ 100 nm wide). The optical-field enhancement, together with the direct interaction between the probe light and the analyte, increased the sensitivity for chemical detection by 50 times when compared to evanescent-wave sensing. This spectrometer distinguished several common organic liquids (e.g., *n*-bromohexane, toluene, isopropanol) accurately and could determine the ratio of chemical species (e.g., acetonitrile and ethanol) at low concentration (<5 μL/mL) in a mixture through spectral scanning over their characteristic absorption peaks in the mid-IR regime. The combination of CMOS-compatible planar mid-IR microphotonics, and a high-throughput nanofluidic sensor system, provides a unique platform for chemical detection.

KEYWORDS: *Midinfrared, opto-nanofluidics, on-chip, sensors*
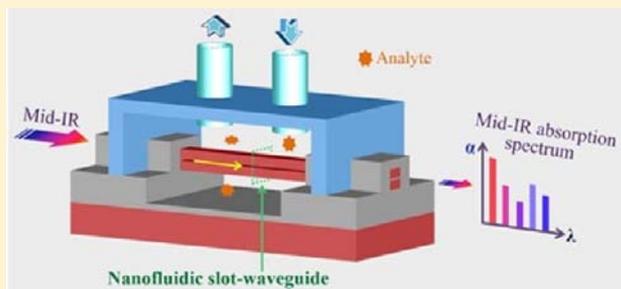
An optofluidic sensor platform that integrates miniature planar microphotonic sensors with high-throughput fluidic circuits could be used for in situ and on-site detection in application such as monitoring urban pollutants, toxins, volatile industrial elements, and certain military threats.[1−4] One major drawback of current optofluidic sensors is the requirement of an additional process of surface functionalization of the optical sensing device in order to identify specific chemicals.[5,6] For instance, biochemical sensors that use shifts in refractive index (e.g., microring resonators and microcavities) can neither differentiate nor identify unlabeled analytes in biological samples effectively without modification of optical sensor surfaces, because many different biochemical species coexist in a biological sample and these species register nearly indistinguishable shifts of refractive index when adsorbed onto the sensors.[7,8] Although resonator-based sensors show high sensitivity at a particular wavelength, broadband and continuous wavelength-swept detection cannot be readily achieved due to the narrow inherent free spectral range (FSR) of these devices.[9,10] As a result, simultaneous monitoring of multiple analytes becomes impractical because a complex array of microfluidic components need to be individually modified with different antibodies or markers.

In contrast to index sensors, mid-infrared spectroscopy is a detection technique commonly used for identifying biochemicals and tracing of toxic molecules[11−15] and is free of target labels and sensor surface functionalization. The use of mid-IR spectrum circumvents the need for labeling the sample, because the characteristic wavelength of absorption by many functional groups present in chemical or biological molecules falls within this region of the spectrum. Current methods for acquiring mid-IR spectra rely on either Fourier transform infrared spectroscopy (FTIR) or a scanning monochromator;[16−20] both methods, however, use benchtop equipment that is too large for hybrid or monolithic chip-scale integration.

Herein, we present a new chip-scale optofluidic device that utilizes mid-IR techniques for label-free and surface functionalization-free chemical sensing. The optofluidic platform is built using CMOS processes and is capable of accomplishing broad mid-IR spectral sensing. Introducing an engineered slot-waveguide into the sensor generates a strong optical field and substantially improves the sensitivity of the device. We

demonstrate experimentally that this mid-IR on-chip sensor can differentiate several organic liquids and can determine the molar fraction of components in a binary mixture of organic liquids at low concentration. With the advantages of lightweight and small footprint, our mid-IR slot-waveguide design can enable the development of sensors for remote, on-site, and body-wearable monitoring of chemicals in the environment.

To realize an optofluidic sensor that can achieve label-free, multianalyte, real-time, and broad spectral tracing, we developed a hybrid chip-scale mid-IR spectrometer that utilized a nanofluidic optical channel. This spectrometer, which has the dimensions of 2 cm (L) × 1 cm (W) × 5 mm (D), is connected to an external tunable laser (60 mW) for identifying multiple chemical functional groups through spectral scanning. Although sophisticated optofluidics has been demonstrated in the visible and near-infrared (NIR) spectrum,[21,22] fingerprint-absorption peaks of organic or biochemical compounds rarely exist in these shorter wavelengths. In contrast, the mid-IR spectrum is particularly useful for chemical analysis because many chemical functional groups have characteristic absorption bands.[23−27] For example, absorption due to C−H bonds of alkyl and aromatic compounds, O−H, and N−H bonds are found within this spectral region.

Advancing optofluidics from the visible/NIR to the mid-IR would require (1) a platform assembled from components transparent to mid-IR radiation and (2) a new approach that can allow the mid-IR probe light to interact with the target analyte efficiently in the fluidic channel.[28−30] This paper describes a mid-IR transparent nanofluidics-based device that utilizes an optical slot-waveguide to confine a broadband mid-IR light wave.[31−34] This device provides improvements over current evanescent-wave detection using fiber- or rib-waveguide in two ways: (1) the availability of a broad spectral range (from $\lambda = 2.5\ \mu$m to $\lambda = 4\ \mu$m) enables the differentiation of multiple chemical species in the same sample; 2) effective spatial confinement of the lightwave in each fluidic channel significantly enhances the interaction between the probe light and the analyte and imparts high sensitivity (<5 μL/mL) to this device.[35−37]

Design Layout of mid-IR Opto-Nanofluidic Platform. Figure 1 schematically illustrates the structure of the mid-IR opto-nanofluidic device. The sensing element is a nanofluidic-channel slot-waveguide (labeled as a fluidic slot-waveguide) with its two ends connected to Si−SiO$_2$−Si slot-waveguides (labeled as a SiO$_2$ slot-waveguide). We embed the entire nanofluidic channel and part of the silicon-oxide slot-waveguides in the center of a chamber made of polydimethylsiloxane (PDMS) and introduce a solution of analyte into the device through plastic tubes that pass through the top of the PDMS chamber. Upon filling the interior of the chamber with liquid analyte, the solution inside the nanofluidic channel converts the fluid-filled channel into a fluidic slot-waveguide. A source of mid-IR probe light is then introduced to the device by direct coupling with one of the two SiO$_2$ slot-waveguides and subsequently enters the fluidic slot-waveguide. The difference in refractive index between SiO$_2$ and the target analyte leads to an optical mode transition at the interface between the SiO$_2$ slot-waveguide and the fluidic slot-waveguide. Our fluidic slot-waveguide, however, encounters minimal optical loss from the mismatch of refractive index during mode transmission because of the similarity in the refractive index of SiO$_2$ ($n_{SiO2} = 1.45$) and common organic liquids ($n = 1.4−1.6$). The nanofluidic channel thus serves two functions in this device: (1) it works as
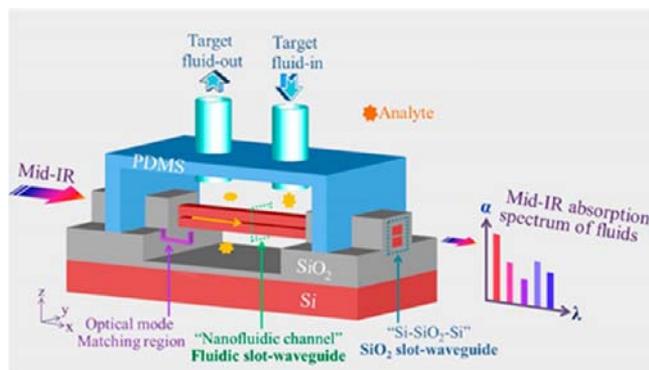

Figure 1. Schematic of a mid-IR opto-nanofluidic sensor composed of (i) a nanofluidic channel with a gap in which fluidic target analytes can fill (labeled as a fluidic slot-waveguide), (ii) a Si−SiO$_2$−Si structure, which acts as an optical mode matching region as well as a mechanical support (labeled as a SiO$_2$ slot-waveguide), and (iii) a PDMS fluidic chamber with an inlet and outlet for delivery of target analytes into and out of the fluidic slot waveguide. Liquid analyte is injected in/out of the chamber through plastic tubes connected to the PDMS chamber. This liquid fills the nanofluidic channel and it is where the optical absorption for spectrum scanning takes place. Mid-IR light is initially coupled into the front SiO$_2$ slot-waveguide and then passes through the optical mode matching region, the fluidic slot waveguide (nanofluidic channel), and finally into the SiO$_2$ slot-waveguide on the exit end. Light transmitted from the waveguide edge encodes the absorption spectrum of the analytes.

a mid-IR waveguide and (2) provides a detection zone that allows maximal spatial overlap between the analyte and the optical field. This interaction between the analyte and the optical field enhances the sensitivity of the device. The two SiO$_2$ slot-waveguides adjacent to the fluidic slot-waveguide seal the two ends of the nanofluidic channel and prevent organic liquid from leaking out the PDMS chamber. Thus, the SiO$_2$ slot-structure serves as (a) an efficient mid-IR medium for transmitting the mid-IR light into and out of the fluidic channel and (b) a fluid-stopping element. After passing through the nanofluidic channel, the mid-IR probe light propagates into the second SiO$_2$ slot-waveguide at the other end. It is subsequently transmitted from the second SiO$_2$ slot-waveguide into free space and is immediately captured and recorded by a mid-IR (InSb) camera detector outside the PDMS chamber. The transmitted light is encoded with the absorption spectrum of the analyte in the fluid because the absorption of probe light by the analyte that fills the nanofluidic channel heavily modulates the intensity of the guided light at the characteristic absorption wavelengths.

To illustrate better the layout of the mid-IR slot-waveguides and their corresponding mid-IR response, we highlight three regimes of the optical cell schematically (Figure 2): the center opto-nanofluidic waveguide and the front and the back Si-SiO$_2$−Si slot waveguides along with the profiles of their refractive index. In either type of waveguides, the center is composed of low-refractive-index medium (SiO$_2$ or organic liquid), while the top and bottom layers are Si strips with a high refractive index of $n_{Si} = 3.45$. According to Maxwell's equation, if a dielectric multilayer has a "High n−Low n−High n" ($n_H−n_L−n_H$) structure, and the n_L layer has subwavelength thickness, high amplitude decaying fields will overlap in the center n_L medium in order to satisfy the continuity of the normal component of electric displacement. As a result, a strong electromagnetic field will be confined and guided by the low-
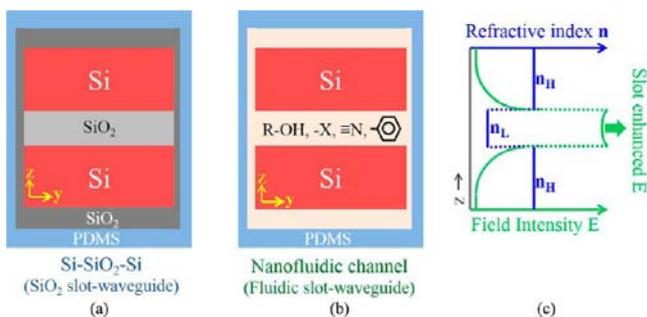
Figure 2. Cross-sectional diagrams of (a) SiO₂ slot-waveguide and (b) nanofluidic channel/fluidic slot-waveguide. (c) The schematic profiles of refractive index and field intensity of a slot-waveguide. (The actual simulated profiles of refractive index and field intensity are illustrated later in Figure 4.) A target analyte, identifiable by its functional group, fills the nanofluidic channel transforming it into a fluidic slot-waveguide. The custom-designed index profile (n_H−n_L−n_H) confines mid-IR light to the fluidic channel, enhancing the interaction time between the target analyte and light.

refractive-index material. On the basis of the same concept, our SiO₂ slot and liquid-core-channel can efficiently guide and confine the mid-IR probe light since both Si−SiO₂−Si and the opto-nanofluidic structures fulfill the n_H−n_L−n_H condition. Furthermore, the full overlap between the fluidic channel and the mid-IR light will improve the chemical sensitivity due to the direct interaction between the enhanced optical field and the analyte. The actual simulated profiles of refractive index and field intensity are illustrated later in Figure 4. In the absence of a slot-structure, only the tail of guided waves (evanescent wave) could interact with analyte, and this configuration would significantly reduce the sensitivity of the device. To avoid absorption of lightwave by PDMS, which is a mid-IR absorptive between λ = 2.6 μm to λ = 4 μm,[38] we introduced an additional SiO₂ layer that conformally covers the Si−SiO₂−Si waveguide to prevent direct contact between the SiO₂ slot-waveguide and the PDMS chamber.

Figure 3 shows micrographs of the fabricated nanofluidic channels and mid-IR slot-waveguides obtained by scanning electron microscope (SEM). On the left, Figure 3a shows an array of SiO₂ slot-waveguides consisting of Si−SiO₂−Si three-layered structures with the top layer fully covered by an extra SiO₂ film, while the right shows several nanofluidic channels. Figure 3b is an enlarged image of the fluidic channel, which has a width of 5 μm, and the image highlights the interface where the optical mode transitions from the SiO₂ slot-waveguide to the fluidic slot-waveguide. To show the topography of the sample, Figure 3c images the sample with a 54° tilt angle. A 5 μm tall conformal SiO₂ layer insulates the Si−SiO₂−Si structure from the PDMS chamber. This structure uniformly covers the underside of the SiO₂ slot-waveguide. Figure 3d shows a nanofluidic channel that is composed of a suspended Si−air−Si structure. The absence of bumps or defects along the channel confirms that its fabrication generated components that have surface characteristics suitable for opto-nanofluidic devices. Figure 3e shows higher-magnification images of a 100 nm thick channel centered between two 1.5 μm thick Si strips. The smooth edges and surfaces of the fluidic slot-waveguides seen in the SEM image are highly desirable for chemical sensing applications as they prevent loss of signal due to light scattering.

The enhancement of chemical sensitivity of our fluidic slot-waveguide is evaluated by simulations using the finite-difference

time-domain (FDTD) and finite-element method (FEM) methods. We determined sensitivity by calculating the attenuation of intensity of a guided wave that passes through a nanofluidic channel filled with mid-IR absorptive fluids. Figure 4a compares the predicted optical-field profiles for propagating mid-IR (λ = 3.3 μm) radiation within a rectangular-strip waveguide to that of a nanofluidic slot waveguide; both waveguides are simulated to be immersed in mid-IR absorptive fluid. The light within the slot waveguide is transverse magnetic (TM) polarized. In the case of the 3 μm tall rectangular strip-waveguide, the optical field is mainly retained inside the Si core and its penetration as an evanescent wave into the surrounding fluid is small. In the slot-waveguide, the optical field is highly concentrated at the center of the fluidic channel and interacts strongly with the liquid inside the channel. Thus, even a slight change in the concentration of analyte will result in a significant modulation of intensity to the guided mid-IR lightwave, which consequently boosts the sensitivity when sensing chemicals. Because the light-confinement inside the slot is dependent on the slot-width d, it is important to evaluate the explicit relationship between d and its associated sensitivity. We define sensitivity-enhancement as S_{slot}/S_{strip}, where S_{slot} and S_{strip} represent the sensitivities of the slot-waveguide and the strip-waveguide, respectively, as depicted in Figure 4a. Figure 4b shows calculated mode profiles at λ = 3300 nm while d gradually increases from 80 to 300 nm. Clearly the mid-IR confinement decreases as the slot become wider. Between d = 80 nm to d = 150 nm a sharp slot waveguide mode is observed. However, as d increases beyond 150 nm a part of mid-IR wave becomes guided by the Si strip instead of the slot. In addition, the field maximum originally found in the slot center splits into two peaks and it also moves to the interfaces between the Si and the slot. As d reaches 300 nm, there is a clear intensity drop in the slot center that results a decrease of sensitivity. Thus, our modeling demonstrates the importance of slot width, for the sensitivity of our mid-IR on-chip sensor. From the plot in Figure 4c, an enhancement-factor S_{slot}/S_{strip} of 56 times is obtained when a slot-structure with d = 300 nm is used, and it rises to 75 times as the slot-width narrows to d = 80 nm. This improvement of sensitivity, arising from the use of a fluidic-slot structure, is attributed to the probe light-confinement within the nanofluidic channel. Although a mid-IR strip waveguide's sensitivity can be improved by reducing waveguide height, the sensitivity enhancement obtained is relatively trivial compared to the enhancement from slot waveguides. From our calculation, the sensitivity of a 2 μm wide × 2 μm high strip waveguide is only 1.5 times greater than a 3 μm wide × 3 μm high strip waveguide, which is far below the 75 times improvement when field concentration effect is introduced from a slot-waveguide. Further reducing the mid-IR strip waveguide size is not practical because it will (a) cause additional waveguide propagation loss (more light will leak into the slightly optical lossy oxide before it enters the opto-fluidic channel) and (b) decrease the mid-IR light coupling efficiency between our 9 μm wide (standard mid-IR) input fiber and the waveguide.

We also investigated the broadband properties of sensitivity-enhancement and the slot-waveguiding strength by calculating the S_{slot}/S_{strip} factor and the effective refractive-index ratio $n_{eff\text{-}slot}/n_{eff\text{-}strip}$, respectively. Figure 4d shows the intensity profiles of mid-IR slot waveguides between wavelengths λ = 3100 nm and λ = 3600 nm, where the slot width d = 100 nm and silicon thickness of 1.5 μm remain constant upon
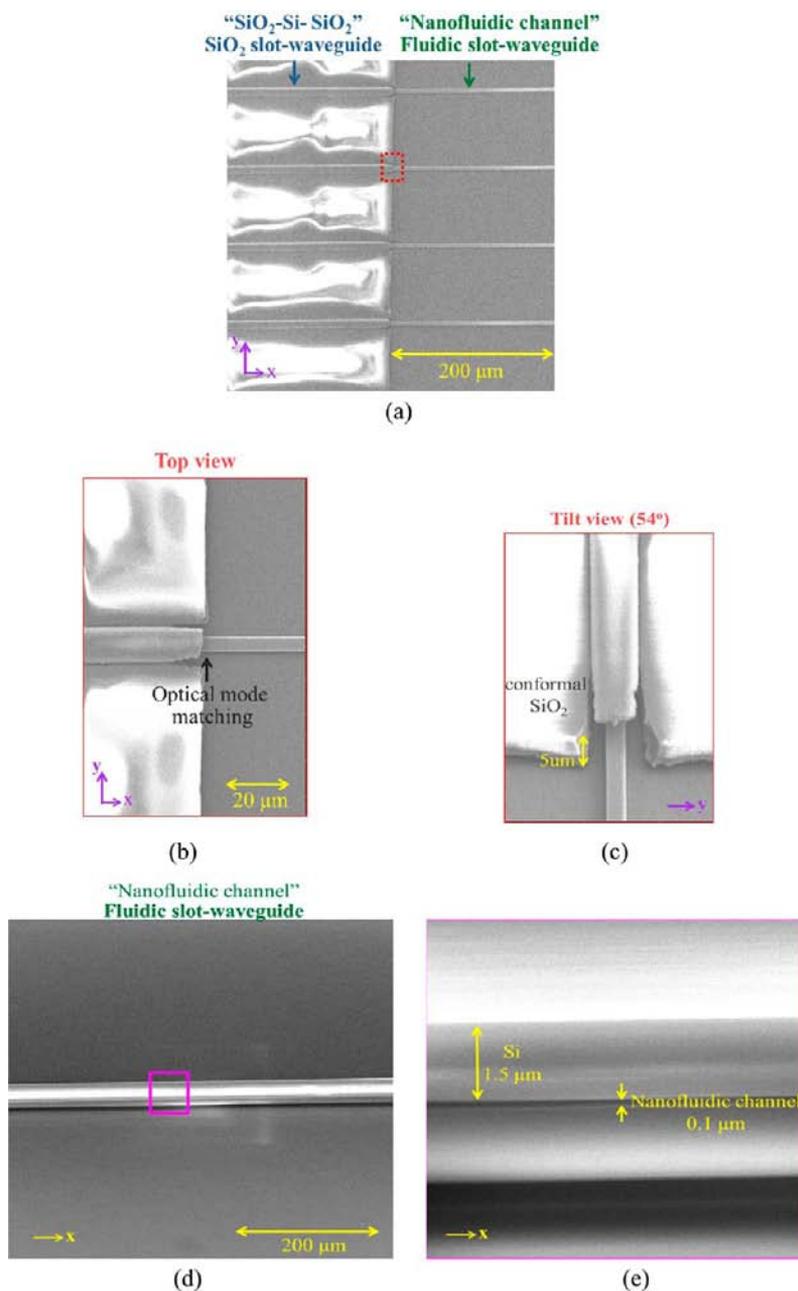
Figure 3. SEM images of the mid-IR spectrometer. (a) An array of "Si–SiO$_2$–Si" SiO$_2$ slot-waveguides (left) and nanofluidic channels (right). The red dashed box indicates the optical mode-matching region. (b) Top view of a magnified image of the mode matching region, showing that the slot-waveguide has a width of 5 μm. (c) Tilted view of the optical mode-matching region. A 5 μm thick conformal layer of SiO$_2$ is seen above the Si–SiO$_2$–Si slot waveguide. (d) Tilted view of a suspended nanofluidic channel. No structural defect is found along the entire channel. (e) Enlarged image of the nanofluidic channel, where a 0.1 μm opening is clearly resolved.

wavelength shift. From the results, mid-IR lightwave is highly confined inside the slot over this broad spectral range, and no significant change is found in the mode profiles. From the plot in Figure 4e, the $S_{\text{slot}}/S_{\text{strip}}$ factors remain constant between $\lambda = 3.1$ μm and $\lambda = 3.6$ μm. This constancy confirms that the enhancement of sensitivity is wavelength independent. Similarly, the $n_{\text{eff-slot}}/n_{\text{eff-strip}}$ ratio has a variation less than 0.05, which implies that the optical mode profile of our slot-waveguide have a negligible difference over a $\Delta\lambda = 0.5$ μm window. Thus, unlike microresonators whose spectral ranges and detection wavelengths are limited by resonance bandwidth and resonant wavelengths, our fluidic slot-waveguides show a wavelength-invariant enhancement of sensitivity and can

perform spectral scanning over a narrow but useful bandwidth; the bandwidth is sufficient for the identification of some molecules and chemical functional groups.

This on-chip mid-IR spectrometer is capable of differentiating compounds with different functional groups and of quantifying the composition of a binary mixture of chemicals. We acquired the absorption spectra by recording the intensity variation of light existing the slot waveguides upon wavelength scan. Figure 5a shows the spectra of *n*-bromohexane, isopropanol, and toluene where distinctive absorption bands were clearly resolved between $\lambda = 3.15$ μm and $\lambda = 3.55$ μm. For *n*-bromohexane, a broad absorption was found at $\lambda = 3.4$ μm, which corresponded to the absorption due to the aliphatic
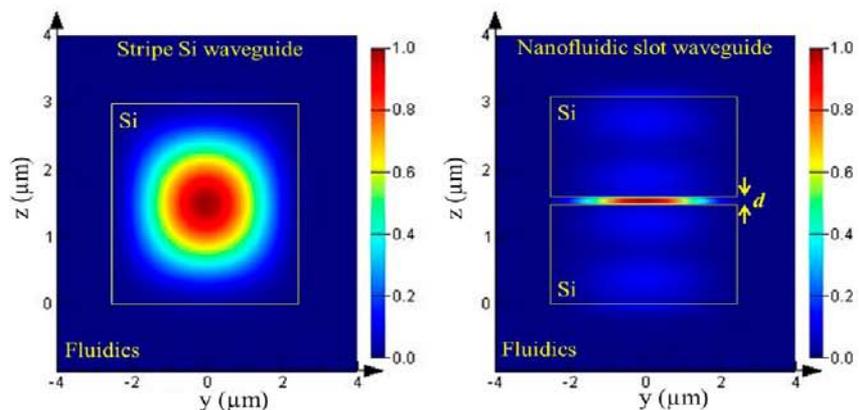
(a)
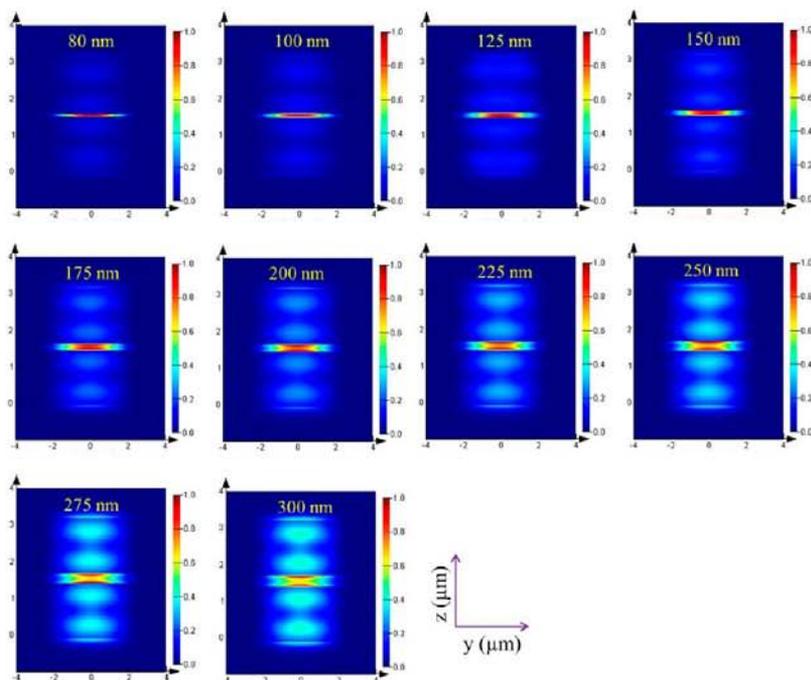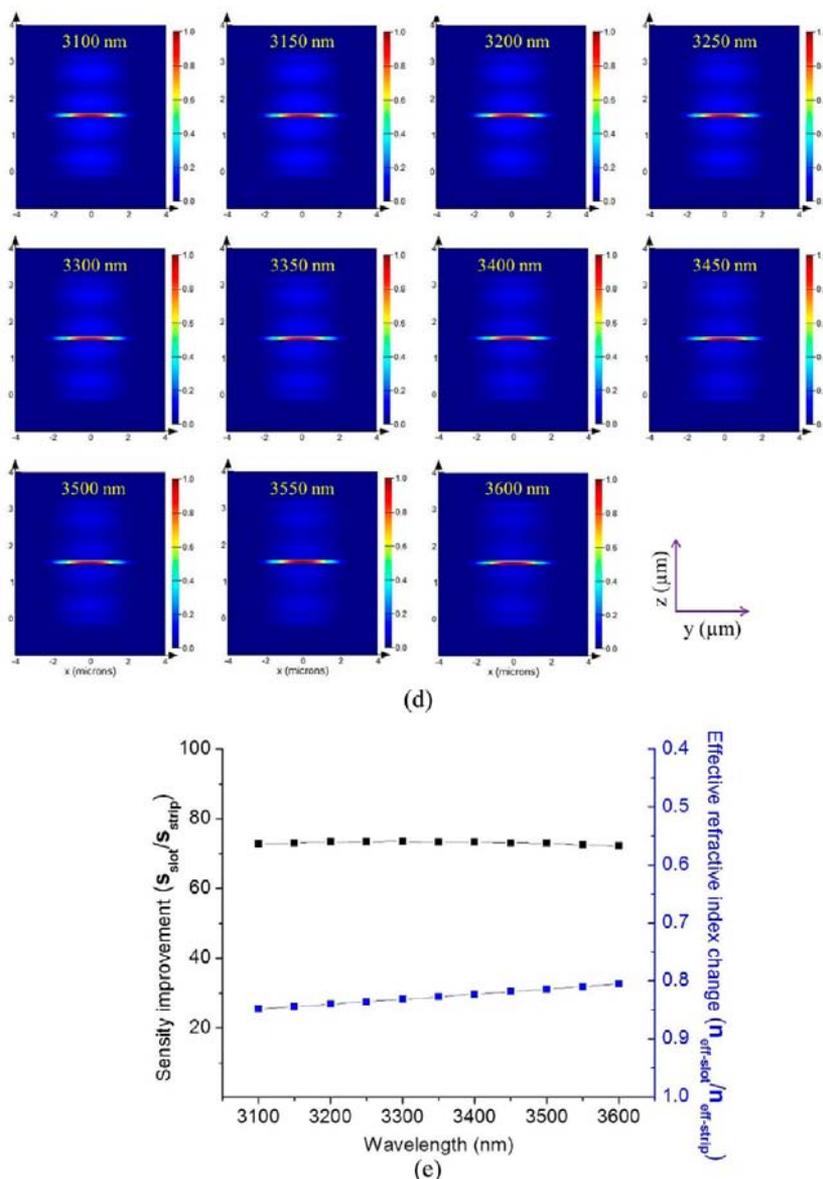

(b)
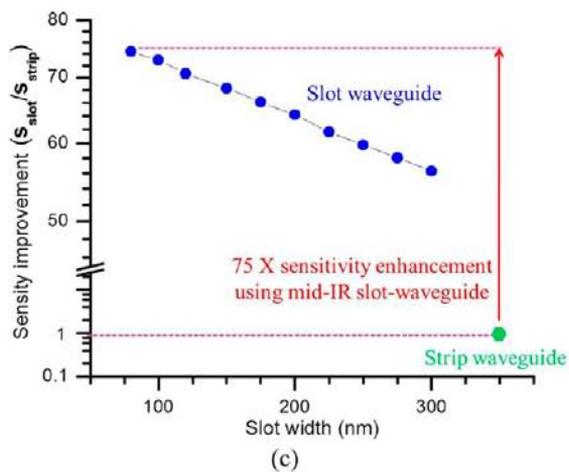
(c)

Figure 4. continued

Figure 4. FDTD and FEM modeling of the nanofluidic slot-waveguides. (a) The field intensity profile of a strip Si waveguide (left) and nanofluidic slot-waveguide (right) at $\lambda = 3300$ nm. For a strip-waveguide, light is guided by the Si medium, whereas strong light confinement inside center fluidic channel is obtained using a slot-waveguide. The color bar indicates the field intensity. (b) Mid-IR slot waveguide modes as slot width d increases from 80 to 300 nm. The wavelength λ is 3300 nm and silicon thickness is 1.5 μm. The intensity of slot waveguide mode decreases and its peak splits into two lobes as the slot width increases. (c) Calculated S_{slot}/S_{strip} ratio (sensitivity improvement) at different slot-width, d. A 75× enhancement is obtained when slot-width d reaches 80 nm. (d) Mid-IR slot waveguide modes as wavelength increases from $\lambda = 3100$ nm to $\lambda = 3600$ nm. The slot width $d = 100$ nm and silicon thickness of 1.5 μm remain constant. No changes of mode profiles are found as the wavelength increases. (e) Calculated S_{slot}/S_{strip} and $n_{eff\text{-}slot}/n_{eff\text{-}strip}$ between $\lambda = 3100$ nm and $\lambda = 3600$ nm. S_{slot}/S_{strip} is wavelength independent and the variation of $n_{eff\text{-}slot}/n_{eff\text{-}strip}$ is less than 5% as the wavelength is swept.

C−H stretches from its long alkyl chain. In the case of isopropanol, two signals were found at $\lambda = 3.15$ μm and $\lambda = 3.4$ μm. The strong intensity absorption below $\lambda = 3.15$ μm was characteristic of O−H stretches, whereas the broad signal at $\lambda = 3.4$ μm was caused by the alkyl C−H stretch. For toluene, multiple peaks were found because it consists of both alkyl and aromatic C−H bonds. The absorption at longer wavelength of $\lambda = 3.4$ μm was attributed to the methyl group while the signals below $\lambda = 3.3$ μm belonged to C−H absorption of the benzene ring. In addition to chemical differentiation, the concentration of compounds in an organic solution of known molecules can also be determined by our mid-IR sensing techniques. To evaluate the improvement in sensitivity, we recorded the optical

intensity profiles transmitted from the mid-IR fluidic-slot waveguide exposed to mixtures of ethanol (EA) and acetonitrile (AN) at different relative concentrations. We chose two wavelengths, $\lambda = 3250$ nm and $\lambda = 3450$ nm, to analyze the composition of the mixtures and the results are shown in Figure 5b. We found that pure ethanol had a higher ratio of intensity ($I_{\lambda=3450 \text{ nm}}/I_{\lambda=3250 \text{ nm}}$) than pure acetonitrile. As the concentration of acetonitrile in ethanol increased, the ratio of intensity at these two wavelengths approached unity. Detailed variation of intensity ratios between different EA/AN compositions are shown in Figure 5c. A sharp drop of $I_{\lambda=3450 \text{ nm}}/I_{\lambda=3250 \text{ nm}}$ is clearly observed as the acetonitrile concentration increased, and we obtained a chemical tracing limit of 10^{-3} volume ratio,
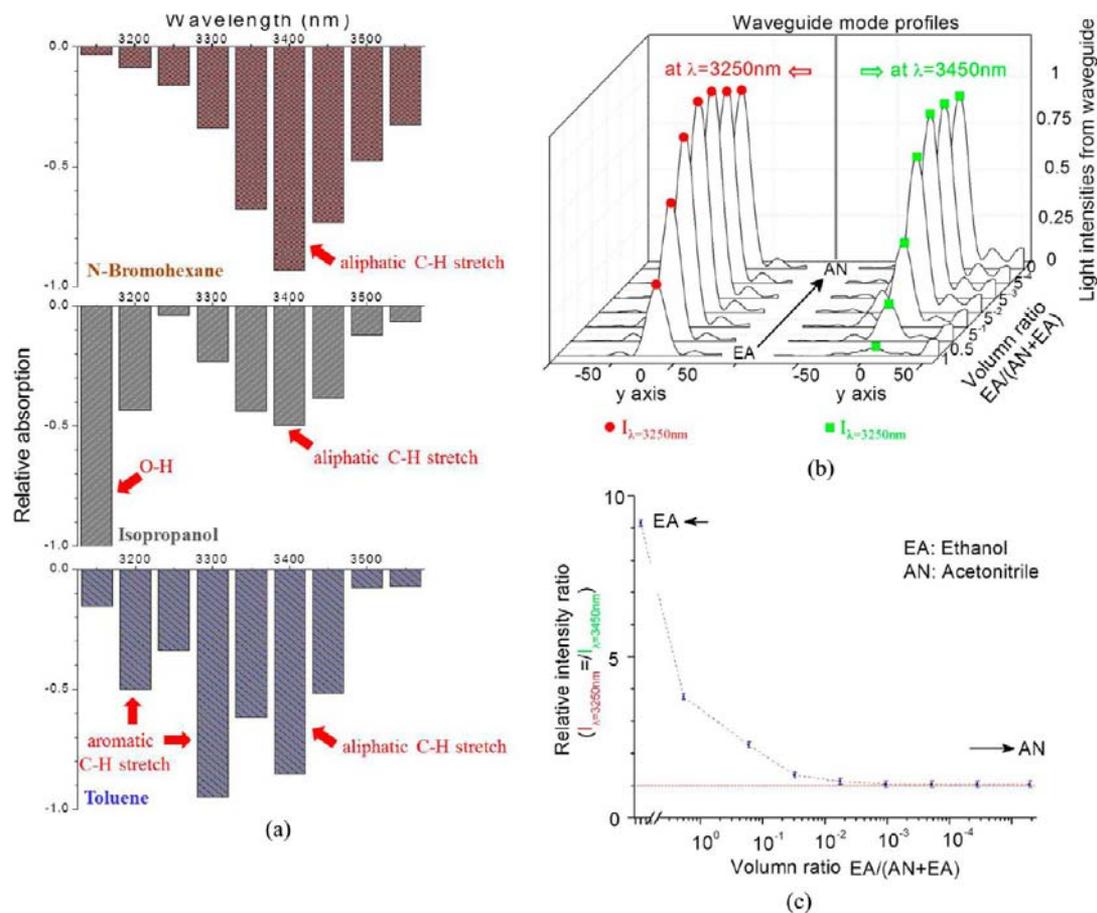
Figure 5. (a) Mid-IR spectrum characterization of *n*-bromohexane, isopropanol, and toluene using our on-chip nanofluidic slot waveguide mid-IR spectrometer. Absorption bands are highlighted and assigned to chemical functional groups. (b) Intensity profiles of waveguide mode along the *y*-axis at λ = 3250 nm (left) and λ = 3450 nm (right) from solutions with different AN/EA volume ratio, where the intensities of peaks, $I_{\lambda=3450}$ nm and $I_{\lambda=3250}$ nm, at different volume ratios are labeled by red circles and green squares respectively. (c) Waveguide intensity ratio between λ = 3250 nm and λ = 3450 nm ($I_{\lambda=3450\ nm}/I_{\lambda=3250\ nm}$) at different EA/AN concentrations. A chemical tracing limit of 5^{-4} is obtained and highlighted by the red line with error bars present.

which was 50 times better than when mid-IR evanescent-wave sensing was used.[39] We attribute the improvement in detection limit to the enhanced direct interaction between the mid-IR light and the analyte and to the efficient light-confinement within a nanofluidic slot-waveguide. The slight deviation of the experimentally observed improvement (50×) from that we modeled (75×) was likely a result of higher-order waveguiding-modes that were simultaneously excited during the light coupling between the fiber and the waveguide.

In conclusion, we have demonstrated a hybrid chip-scale integrated mid-IR spectrometer that can achieve label-free and surface-functionalization-free chemical identification of several compounds. Our sensor can also detect the concentration of solutions. The miniaturized chemical sensor integrates opto-nanofluidics with engineered slot-waveguides, and it achieves optical-waveguide mode-matching. Owing to direct interaction of light with sample and strong nanoscale light-confinement a 50 times enhancement of sensitivity over a strip-waveguide evanescent-wave based optofluidic sensor device is accomplished. We experimentally demonstrated the ability to differentiate *n*-bromohexane (R−Br), isopropanol (R−OH), and toluene (Ar−CH$_3$) by associating the spectral light intensity with characteristic mid-IR absorption. Our mid-IR opto-nanofluidics platform establishes a new approach in

developing compact, high throughput, and in-field chemical monitoring.

■ ASSOCIATED CONTENT

Ⓢ Supporting Information

Fabrication of mid-IR slot waveguides and nanofluidic channels and experimental setup for on-chip mid-IR spectrum characterization. This material is available free of charge via the Internet at http://pubs.acs.org.

■ AUTHOR INFORMATION

Corresponding Author

*E-mail: paolin@mit.edu.

Author Contributions

Device preparation: P.T. L., S.W.K, and H.-Y.G.L. Device design: P.T.L, S.W.K, and H.-Y.G.L. Mid-IR characterization: P.T. L. and V.S. Data analysis: P.T.L, S.W.K, H.-Y.G.L., G.M.W., and A.A. Modeling: P.T. L. and V.S. Writing: P.T.L., A.A., S.W.K., and G.M.W. Project planning: L.C.K., G.M.W., and A.A.

Notes

The authors declare no competing financial interest.

REFERENCES

(1) Gervais, L.; Rooij, N. d.; Delamarche, E. *Adv. Mater.* **2011**, *23*, H151–H176.

(2) Sloan, C. D. K.; Marty, M. T.; Sligar, S. G.; Bailey, R. C. *Anal. Chem.* **2013**, *85*, 2970–2976.

(3) Chen, Y.-F.; Jiang, L.; Mancuso, M.; Jain, A.; Oncescuc, V.; Erickson, D. *Nanoscale* **2012**, *4*, 4839–4857.

(4) Whitesides, G. M. *Nature* **2006**, *442*, 368–373.

(5) Ng, A. H. C.; Uddayasankar, U.; Wheeler, A. R. *Anal. Bioanal. Chem.* **2010**, *397*, 991–1007.

(6) Shia, W. W.; Bailey, R. C. *Anal. Chem.* **2013**, *85*, 805–810.

(7) Zuta, Y.; Goykhman, I.; Desiatov, B.; Levy, U. *Opt. Express* **2010**, *18*, 24762–24769.

(8) Luchansky, M. S.; Bailey, R. C. *J. Am. Chem. Soc.* **2011**, *133*, 20500–20506.

(9) Mandal, S.; Erickson, D. *Opt. Express* **2008**, *16*, 1623–1631.

(10) Huang, M.; Yanik, A. A.; Chang, T.-Y.; Altug, H. *Opt. Express* **2009**, *17*, 24224–24233.

(11) Dam, J. S.; Tidemand-Lichtenberg, P.; Pedersen, C. *Nat. Photonics* **2012**, *6*, 788–793.

(12) Naumann, D.; Helm, D.; Labischinski, H. *Nature* **1991**, *351*, 81–82.

(13) Nasse, M. J.; Walsh, M. J.; Mattson, E. C.; Reininger, R.; Kajdacsy-Balla, A.; Macias, V.; Bhargava, R.; Hirschmugl, C. J. *Nat. Methods* **2011**, *8*, 413–416.

(14) Ataka, K.; Kottke, T.; Heberle, J. *Angew. Chem., Int. Ed.* **2010**, *49*, 5416–5424.

(15) Sathyanarayana, D. N. *Vibrational Spectroscopy: Theory and Applications*; New Age International, New Delhi, India, 2007.

(16) Griffiths, P. R.; de Haseth, J. A. *Fourier Transform Infrared Spectrometry*, 2nd ed.; John Wiley & Sons: New York, 2007.

(17) Bhargava, R.; Levin, I. W. *Anal. Chem.* **2001**, *73*, 5157–5167.

(18) Fernandez, D. C.; Bhargava, R.; Hewitt, S. M.; Levin, I. W. *Nat. Biotechnol.* **2005**, *23*, 469–474.

(19) Zhu, J.; Mathes, T.; Stahl, A. D.; Kennis, J. T. M.; Groot, M. L. *Opt. Express* **2012**, *20*, 10562–10571.

(20) Baxter, J. *Nat. Photonics* **2012**, *6*, 412–412.

(21) Psaltis, D.; Quake, S. R.; Yang, C. *Nature* **2006**, *442*, 381–386.

(22) Testa, G.; Huang, Y.; Sarro, P. M.; Zeni, L.; Bernini, R. *Appl. Phys. Lett.* **2010**, *97*, 131110.

(23) Dam, J. S.; Tidemand-Lichtenberg, P.; Pedersen, C. *Nat. Photonics* **2012**, *6*, 788–793.

(24) Naumann, D.; Helm, D.; Labischinski, H. *Nature* **1991**, *351*, 81–82.

(25) Nasse, M. J.; Walsh, M. J.; Mattson, E. C.; Reininger, R.; Kajdacsy-Balla, A.; Macias, V.; Bhargava, R.; Hirschmugl, C. J. *Nat. Methods* **2011**, *8*, 413–416.

(26) Ataka, K.; Kottke, T.; Heberle, J. *Angew. Chem., Int. Ed.* **2010**, *49*, 5416–5424.

(27) Chalmers, J. M.; Griffiths, P. R. *Handbook of Vibrational Spectroscopy*; Wiley: New York, 2002.

(28) Lin, P. T.; Singh, V.; Lin, H.-Y. G.; Tiwald, T.; Kimerling, L. C.; Agarwal, A. M. *Adv. Opt. Mater.* **2013**, DOI: 10.1002/adom.201300205.

(29) Lin, P. T.; Singh, V.; Kimerling, L. C.; Agarwal, A. M. *Appl. Phys. Lett.* **2013**, *102*, 251121.

(30) Lin, P. T; Singh, V.; Cai, Y.; Kimerling, L. C.; Agarwal, A. *Opt. Lett.* **2013**, *7*, 1031.

(31) Sun, R.; Dong, P.; Feng, N.-N.; Hong, C.-Y.; Michel, J.; Lipson, M.; Kimerling, L. *Opt. Express* **2007**, *15*, 17967–17972.

(32) Preston, K.; Lipson, M. *Opt. Express* **2009**, *17*, 1527–1534.

(33) Yang, A. H. J.; Moore, S. D.; Schmidt, B. S.; Klug, M.; Lipson, M.; Erickson, D. Optical manipulation of nanoparticles and biomolecules in sub-wavelength slot waveguides. *Nature* **2009**, *457*, 71–75.

(34) Ramírez, J. M.; Lupi, F. F.; Berenćen, Y.; Anopchenko, A.; Colonna, J. P.; Jambois, O.; Fedeli, J.; M. Pavesi, L.; Prtljaga, N.; Rivallin, P.; Tengattini, A.; Navarro-Urrios, D.; Garrido, B. *Nanotechnology* **2013**, *24*, 115202.

(35) Fei, P.; Chen, Z.; Men, Y.; Li, A.; Shenac, Y.; Huang, Y. *Lab Chip* **2012**, *12*, 3700–3706.

(36) Schmidt, H.; Hawkins, A. R. *Nat. Photonics* **2011**, *5*, 598–604.

(37) Gopalakrishnan, N.; Sagar, K. S.; Christiansen, M. B.; Vigild, M. E.; Ndoni, S.; Kristensen, A. *Opt. Express* **2010**, *18*, 12903–12908.

(38) He, T.; Liang, Q.; Zhang, K.; Mu, X.; Luo, T.; Wang, Y.; Luo, G. *Microfluid. Nanofluid.* **2011**, *10*, 1289–1298.

(39) Lin, P. T.; Singh, V.; Hu, J.; Richardson, K.; Musgraves, J. D.; Luzinov, I.; Hensley, J.; Kimerling, L. C.; Agarwal, A. *Lab Chip* **2013**, *13*, 2161–2166.